

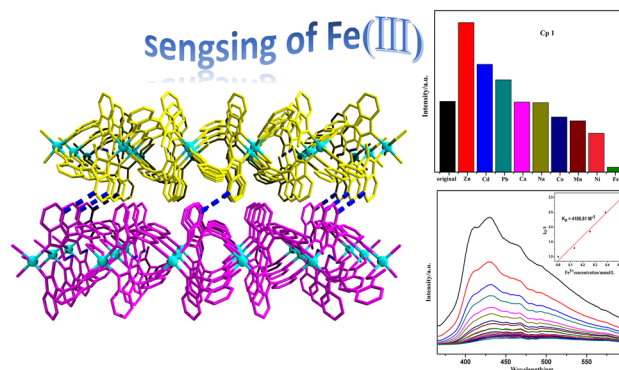
Two 1D Looped Coordination Polymers as Luminescent Probes for Highly Selective Sensing of Fe³⁺ Ions

Yan-Ping Fan¹ · Yi-Fan Kang² · Xi-Qiang Liang³ · Quan-Quan Li¹ · Wen-Qian Zhang¹ · Ping Liu¹ · Yao-Yu Wang¹

Received: 14 March 2017 / Accepted: 23 May 2017 / Published online: 6 June 2017
© Springer Science+Business Media New York 2017

Abstract Two luminescent coordination polymers (LCPs), namely [CdL₂]_n (**1**) and [ZnL₂]_n (**2**) based on a new ligand 2-(2-methyl-benzimidazole-1-yl)-benzoic acid (HL), have been synthesized and characterized by single crystal X-ray diffraction, powder X-ray diffraction, infrared spectroscopy, elemental analysis, and thermogravimetric analysis. **1** and **2** exhibit similar 1D looped chains with different coordination modes of L. Both LCPs show strong fluorescent emission in the visible region. The fluorescence quenching response of **1** and **2** towards Fe³⁺ over other metal ions in DMF has been demonstrated by quenching titrations. Thus, **1** and **2** can be used as potential and highly selective luminescent sensors for Fe³⁺ ions.

Graphical Abstract



Keywords Luminescent coordination polymers · 1D looped chains · Thermostability · Fluorescent probes · Fe³⁺

1 Introduction

Iron is one of the most important elements in the metabolic process for all living system [1]. The deficiency or excess of the iron element relative to the normal limits could induce serious diseases, such as Alzheimer's, Huntington's or Parkinson's disease [2]. The considerable importance of iron in biological systems has promoted the development of methods to selectively detect and quantify Fe³⁺. However, most traditional analytical techniques for detecting Fe³⁺, including spectrophotometry, atomic absorption spectrometry and chromatography, are time-consuming, labor-intensive or indirect-viewed [3, 4]. In recent years, luminescent chemical sensors have emerged as reliable alternatives for detection of metal ions, [5–7] which are technologically friendly, easy to integrate to the existing infrastructures, have a low detection limit, and can selectively identify

Electronic supplementary material The online version of this article (doi:10.1007/s10904-017-0591-z) contains supplementary material, which is available to authorized users.

✉ Ping Liu
liuping@nwu.edu.cn

- 1 College of Chemistry & Materials Science, Northwest University, Xi'an 710127, China
- 2 College of Chemistry & Chemical Engineering, Shaanxi University of Science and Technology, Xi'an 710021, China
- 3 Department of Laboratory Medicine, Xi'an Children Hospital, Xi'an 710003, Shaanxi, China

targeted molecules. In particular, they have potential applications in analytical chemistry and biomedical diagnostic [8–11].

The ability of luminescent coordination polymers (LCPs) to propagate the host guest interaction to detectable changes as a function of their luminescence makes them promising candidates for sensing metal ions. LCPs have several advantages including simple one-pot and straightforward synthesis, remarkable structural tailorability and functionalizability as well as their enormous practical applications, such as biomedical assays and time-resolved microscopy, fluorescent lighting, and luminescent sensing for chemical species [7, 10, 12, 13]. Therefore, efforts have been made to cultivate LCPs to detect metal ions and explore sensing mechanisms [14–16]. Generally, the detection process of metal ions is primarily based on fluorescence quenching via donor–acceptor electron transfer, resonance energy transfer or structural damage mechanism [17–19].

It is well-known that many benzimidazole and its derivatives have been used as efficient fluorophores, which have high fluorescence quantum yields, large Stokes shifts, and excellent coordination ability with transition metals [20]. For example, according to Barnard, benzimidazole derivatives can be used as carbene precursors to construct carbene complexes with good fluorescent properties [21]. Moreover, benzimidazole and its derivatives can also be considered as ligands to build LCPs. Zhang's group has reported Cu(I) compounds, in which the alteration of Cu···Cu and π ··· π interactions in the structure, may lead to luminescent changes [22]. The luminescence of Mg-based and Zn-based LCPs reported by Zheng occurs a significant red shift compared with ligand, which is probably due to the ligand-to-metal charge-transfer (LMCT) transition [23]. Based on these reasons, the 2-(2-methyl-benzimidazole-1-yl)-benzoic acid (HL) ligand is selected to build LCPs with the following characteristic features: (1) carboxylic group easily participate in coordination, and form various complexes with variable coordination modes; [24] (2) N atoms from benzimidazole moiety also can coordinate with metal ions by providing lone electron pairs; [25] (3) there is a large steric hindrance between carboxylic group and methyl from *o*-substituted 2-methyl-benzimidazole moiety, so there exist a relatively large twist angle; [26] (4) large π electronic systems will change the fluorescence properties; [27] (5) up to now, this ligand has not been investigated to construct complexes. Herein, based on HL, we report two 1D looped LCPs, namely, $[\text{CdL}_2]_n$ (**1**) and $[\text{ZnL}_2]_n$ (**2**). The crystal structures, infrared (IR) spectra, thermogravimetric analysis (TGA), luminescent spectra and fluorescent sensing for Fe^{3+} were investigated. Both LCPs exhibit high thermostability up to 330 and 350 °C, respectively. The most striking phenomenon is that Fe^{3+} ion causes a very significant

quenching effect on luminescence of **1** and **2**. Thus, **1** and **2** can be used as potential and highly selective luminescent sensors for Fe^{3+} ions. In addition, a possible sensing mechanism for both LCPs is also discussed.

2 Experimental

2.1 Materials and Equipment

All chemicals were available commercially (HL was purchased from Jinan Henghua Science & Technology Co., Ltd.) and utilized without further purification. The C, H and N microanalyses were carried out with a Perkin–Elmer 2400 C elemental analyzer. IR spectrum was recorded from KBr pellets in the 4000–400 cm^{-1} range on a Nicolet Avatar 360 FTIR spectrometer. TGA were performed on a Netzsch TG209F3 equipment (30–700, 10 °C min^{-1} , N_2 gas flow). The powder X-ray diffraction (PXRD) was recorded in the angular range of $2\theta = 5$ – 50° with a Bruker D8 ADVANCE X-ray powder diffractometer (Cu-K α , 1.5418 Å). Luminescence spectra for the solid samples and liquid samples were taken with a Perkin–Elmer LS55 luminescence spectrometer. UV–Vis spectroscopic studies were measured on a Hitachi U-3310 spectrometer.

2.2 Syntheses

2.2.1 Preparation of $[\text{CdL}_2]_n$ (**1**)

A mixture of the HL (0.0252 g, 0.1 mmol) and $\text{Cd}(\text{OAc})_2 \cdot 2\text{H}_2\text{O}$ (0.0131 g, 0.05 mmol) in NMP (N-methyl-2-pyrrolidone)/ H_2O (2/8, 10 mL) was placed in a Parr Teflon-lined stainless steel vessel and heated to 105 °C for 3 days. After the mixture was cooled to room temperature at the rate of 0.1 °C min^{-1} , the colorless crystals of **1** were collected to give 68% yield based on HL. Anal. Calcd for **1** ($M_r = 307.47 \text{ g mol}^{-1}$): C, 58.59; H, 3.57; N, 9.10%. Found: C, 58.52; H, 3.49; N, 9.06%. IR (cm^{-1} , KBr pellet): 3436 (w), 1593 (s), 1556 (s), 1500 (m), 1457 (w), 1390 (s), 1324 (w), 1032 (w), 845 (w), 745 (m).

2.2.2 Preparation of $[\text{ZnL}_2]_n$ (**2**)

A mixture of the HL (0.0252 g, 0.1 mmol) and $\text{Zn}(\text{OAc})_2 \cdot 2\text{H}_2\text{O}$ (0.0110 g, 0.05 mmol) in $\text{CH}_3\text{CN}/\text{H}_2\text{O}$ (2/8, 10 mL) was placed in a Parr Teflon-lined stainless steel vessel and heated to 120 °C for 3 days. After the mixture was cooled to room temperature at the rate of 0.1 °C min^{-1} , the colorless crystals of **2** were collected to give 36% yield based on HL. Anal. Calcd for **2** ($M_r = 283.94 \text{ g mol}^{-1}$): C, 63.39; H, 3.87; N, 9.86%. Found: C, 63.32; H, 3.85; N, 9.80%. IR (cm^{-1} , KBr

pellet): 3450 (*w*), 1629 (*s*), 1500 (*m*), 1457 (*w*), 1405 (*w*), 1354 (*s*), 1032 (*w*), 845 (*w*), 742 (*m*).

2.3 X-ray Crystallography

Crystallographic data of the LCPs were collected on a Bruker SMART APEX II CCD diffractometer equipped with a graphite monochromated Mo-K α radiation ($\lambda = 0.71073$ Å) at room temperature. The structures were solved by direct methods and refined on F_2 via the full-matrix least-squares technique by applying the program SHELX-97 [28, 29]. All the non-hydrogen atoms have suffered from the anisotropic refinement. And all hydrogen atoms were located in the architectural calculation at desired positions with a riding model and refined isotropically. Crystallographic data and experimental details for structural analyses are shown in Table 1. Selected bond lengths and bond angles are listed in Table 2. The CCDC: 1521923 and 1521924 for **1** and **2**.

Table 1 Crystallographic data and structure refinement parameters for **1** and **2**

LCPs	1	2
Empirical formula	C ₃₀ H ₂₂ N ₄ O ₄ Cd	C ₃₀ H ₂₂ N ₄ O ₄ Zn
Formula weight	614.92	567.89
Crystal shape	block	block
Crystal color	colorless	colorless
Wavelength/Å	0.71073	0.71073
Crystal system	Orthorhombic	Orthorhombic
Space group	<i>Pccn</i>	<i>Pccn</i>
<i>a</i> /Å	23.141 (4)	22.789 (1)
<i>b</i> /Å	7.9209 (1)	7.921 (4)
<i>c</i> /Å	14.288 (2)	14.510 (7)
β /°	90	90
<i>V</i> /Å ³	2619 (7)	2619 (2)
<i>T</i> /K	296 (2)	296 (2)
<i>Z</i>	4	4
<i>D_c</i> /mg m ⁻³	1.560	1.440
μ /mm ⁻¹	0.878	0.982
<i>F</i> (000)	1240	1168
Max. Min. transmission	0.8371, 0.8236	0.8130, 0.7914
Reflections collected	15,673	15,709
Data/restraints/parameters	3479, 0, 178	3432, 1, 178
R_1^a, wR_2^b [$I > 2\sigma(I)$]	0.0359, 0.0996	0.0545, 0.1188
R_1^a, wR_2^b (all data)	0.0734, 0.1374	0.1234, 0.1520

$$^a R_1 = \sum \|F_o - F_c\| / \sum F_o$$

$$^b wR_2 = \sum [\omega(F_o^2 - F_c^2)^2] / \sum [\omega(F_o^2)^2]^{1/2}$$

3 Results and Discussion

3.1 Crystal Structure Description

1 crystallizes in the orthorhombic *pccn* space group, showing a 1D looped chain. There are a half of Cd(II) ions, one L ligand in the asymmetric unit (Fig. 1a). The six-coordinated Cd(II) locates in a distorted octahedral coordination environment [CdN₂O₄], tightly bonded by four O atoms from two chelate coordinated carboxylic groups of two L ligands and two N atoms from another two L ligands. The Cd–O bond lengths are 2.261(3) and 2.516(3) Å and Cd–N bond length is 2.320(3) Å, which are in accordance with those in other related articles [30]. Each Cd(II) ion is bonded to two adjacent Cd(II) ions through two pairs of bridging L, to constitute an infinite

1D double chain parallel to *c* axis (Fig. 1c) with the neighboring interchain Cd⋯Cd separation being 7.144(3) Å. A 3D supramolecular architecture constructed from the 1D chain is stabilized by the hydrogen bonding interactions C9–H9⋯C9 and C15–H15⋯C15 (Fig. 1d). The dihedral angle between benzene ring and benzimidazole moiety is ca. 70° (Fig. S1).

The single crystal X-ray analysis reveals that structures of **1** and **2** are similar. However, some differences still exist. In **2**, each Zn(II) ion is four-coordinated with two monodentate coordinated carboxylic oxygens and two benzimidazole nitrogen donors from four distinct L ligands to furnish a distorted tetrahedral coordination geometry [ZnN₂O₂] (Fig. 1b). The reasons for the change of coordination modes of carboxyl from chelate in **1** to monodentate in **2** may include: (1) Zn⋯O2 separation (2.867(2) Å) exceeds the Zn–O normal distance [31, 32]. (2) The radius of Cd(II) is larger than that of Zn(II), thus Cd(II) can connect more active atoms, resulting in different coordination modes. The Zn–O and Zn–N bond lengths are 1.949(3) and 2.065(3) Å, well comparable to the reported values [33]. The neighboring interchain Zn–Zn separation is 7.255(2) Å. The dihedral angle between benzene ring and benzimidazole moiety is ca. 72° (Fig. S1).

3.2 The PXRD and IR Spectra

PXRD patterns for **1** and **2** were measured on bulk crystalline powders to identify the phase purity of the product. The experimental PXRD patterns of **1** and **2** are in good agreement with simulated ones, respectively, demonstrating the consistency of as-synthesized bulk samples and the testing single crystals (Fig. S2). The discrimination of intensity might be owing to the powder samples' preferred orientation. The IR spectra of **1** and **2** display the characteristic asymmetric (ν_{as}) and symmetric (ν_s) stretching vibrations of the carboxylate groups (Fig. S3). The difference

Table 2 The selected bond lengths (Å) and angles (°) for LCPs **1** and **2**

1			
Cd(1)–O(1)#2	2.516 (3)	Cd(1)–O(2)#2	2.261 (3)
Cd(1)–O(2)	2.261 (3)	Cd(1)–O(1)	2.516 (3)
Cd(1)–N(1)	2.320 (3)	Cd(1)–N(1)#2	2.320 (3)
O(2)–Cd(1)–O(2)#2	162.44 (1)	O(2)–Cd(1)–N(1)#2	90.95 (1)
O(2)#2–Cd(1)–N(1)#2	100.86 (1)	O(2)–Cd(1)–N(1)	100.86 (1)
O(2)#2–Cd(1)–N(1)	90.95 (1)	N(1)#2–Cd(1)–N(1)	95.63 (1)
O(2)–Cd(1)–O(1)	53.93 (1)	O(2)#2–Cd(1)–O(1)	111.81 (1)
N(1)#2–Cd(1)–O(1)	144.01 (1)	N(1)–Cd(1)–O(1)	98.43 (1)
O(2)–Cd(1)–O(1)#2	111.81 (1)	O(2)#2–Cd(1)–O(1)#2	53.93 (1)
N(1)#2–Cd(1)–O(1)#2	98.43 (1)	N(1)–Cd(1)–O(1)#2	144.01 (1)
O(1)–Cd(1)–O(1)#2	89.28 (1)		
2			
N(1)–Zn(1)	2.065 (3)	O(1)–Zn(1)	1.949 (3)
Zn(1)–O(1)#2	1.949 (3)	Zn(1)–N(1)#3	2.065 (3)
Zn(1)–N(1)#1	2.008 (8)		
O(1)–Zn(1)–N(1)#3	99.79 (1)	O(1)#2–Zn(1)–N(1)#3	106.35 (1)
O(1)–Zn(1)–N(1)#1	106.35 (1)	O(1)#2–Zn(1)–N(1)#1	99.79 (1)
N(1)#3–Zn(1)–N(1)#1	102.89 (1)	O(1)–Zn(1)–O(1)#2	137.52 (1)

Symmetry codes: For **1**, #2 $-x+1/2, -y+1/2, z$; For **2**, #1 $x, -y+3/2, z+1/2$; #2 $-x+1/2, -y+3/2, z$; #3 $-x+1/2, y, z+1/2$

($\Delta = \nu_{as} - \nu_s$) between ν_{as} and ν_s has been widely used as a diagnosis of the coordination modes of the carboxylate group. In **1** and **2**, the $\nu_{as}(\text{COO}^-)$ vibration appears at 1593 and 1629 cm^{-1} , and $\nu_s(\text{COO}^-)$ vibration appears at 1393 and 1354 cm^{-1} , respectively. The intermediate Δ value [200 cm^{-1} (**1**) and 275 cm^{-1} (**2**)] is consistent with the chelating and monodentate coordination modes of the carboxylate group [34]. Absorption bands at 1500 cm^{-1} are due to C=C of ligand stretching vibrations. In addition, the spectra of the **1** and **2** show bands at 1032 and 1457 cm^{-1} due to the C–N and C=N stretching modes of the benzimidazole-1-yl ligands [35]. The absence of any strong absorption bands around 1720–1690 cm^{-1} confirms the complete deprotonation of the carboxyl groups of the HL ligands during the reactions [36].

3.3 Thermogravimetric Analysis

TGA were performed to determine the thermal stability of **1** and **2**. The TGA was carried out in the temperature range of 30–700 °C under a flow of nitrogen atmosphere with a heating rate of 10 °C min^{-1} (Fig. 2). TGA curves of **1** and **2** had no obvious weight loss before 330 and 350 °C,

respectively, indicating high thermostability. And then an obvious weight loss of 14.40% for **1** (15.39% for **2**) from 330 to 370 °C (from 350 to 490 °C for **2**) were observed, corresponding to the release of carboxyl moiety (14.31% for **1**, and 15.49% for **2**). The further heating led to the structural collapse, while the remaining weight corresponds to CdO for **1** (obsd 41.72%, calcd 41.76%). For **2**, the remaining weight observed was 66.04%, which was more than 28.66% (the residue is ZnO) less than 78.93% (the residue is Zn_3N_2), corresponding to mixture of ZnO and Zn_3N_2 , but the specific ratio of mixture cannot be obtained because of limited ability.

3.4 Luminescent Properties

The excitation and emission spectra of LCPs **1**, **2** and ligand in the solid-state at room temperature are shown in Fig. 3. It can be seen that ligand display an intense emission band at 415 nm upon excitation at 355 nm, which may be attributed to the $\pi^* \rightarrow n$ or $\pi^* \rightarrow \pi$ transition as previously reported [37]. Interestingly, **1** and **2** exhibit the maximum emission at 435 nm, excited at 340 nm. Compared to the ligand, **1** and **2** indeed result in a large red shift of 20 nm for maximum emission, which indicates that the emission of **1** and **2** at 435 nm may have originated from ligand to metal charge-transfer transitions [38–40]. The red shift can be attributed to coordination of the ligands to metal ions which effectively increases the rigidity of the ligands and reduced the loss of energy via radiation less thermal vibration decay [41–43].

The crystalline samples of **1** and **2** are stable in air and insoluble in common solvents such as DMF, DMA, NMP, CH_2Cl_2 , CH_3OH , $\text{CH}_3\text{CH}_2\text{OH}$, DMSO, CH_3CN and H_2O . In order to examine the potential application of **1** and **2** in sensing cations, **1/2** (5 mg) was immersed in DMF solutions (3 mL) of metal ions (5 mg, $\text{Zn}(\text{NO}_3)_2$, $\text{Cd}(\text{NO}_3)_2$, $\text{Pb}(\text{NO}_3)_2$, $\text{Ca}(\text{NO}_3)_2$, NaNO_3 , $\text{Co}(\text{NO}_3)_2$, $\text{Mn}(\text{NO}_3)_2$, $\text{Ni}(\text{NO}_3)_2$ and $\text{Fe}(\text{NO}_3)_3$), treated by ultrasonication for 30 min, and then aged for 1 h to generate stable suspensions before the fluorescence study. Naturally, the luminescent properties of **1** and **2** in different metal ions suspensions are measured. Interestingly, it was found that Cd^{2+} , Zn^{2+} , Pb^{2+} ions slightly enhanced luminescence intensity of **1** and **2**, while Na^+ , Ca^{2+} ions had a trivial effect on the luminescence intensity, other metal ions (Co^{2+} , Ni^{2+} , Mn^{2+}) decreased luminescence to a different extent. The most striking phenomenon is that Fe^{3+} ion can almost completely quench to the system (Fig. 4a). The obvious change of luminescent intensities implies that **1** and **2** can be considered as a promising candidate for selective probing of Fe^{3+} . The PXRD patterns conform that the framework of **1** and **2** immersed in metal ion solutions remains unchanged (Fig. S4). Fe^{3+} shows strong absorption from 200 to

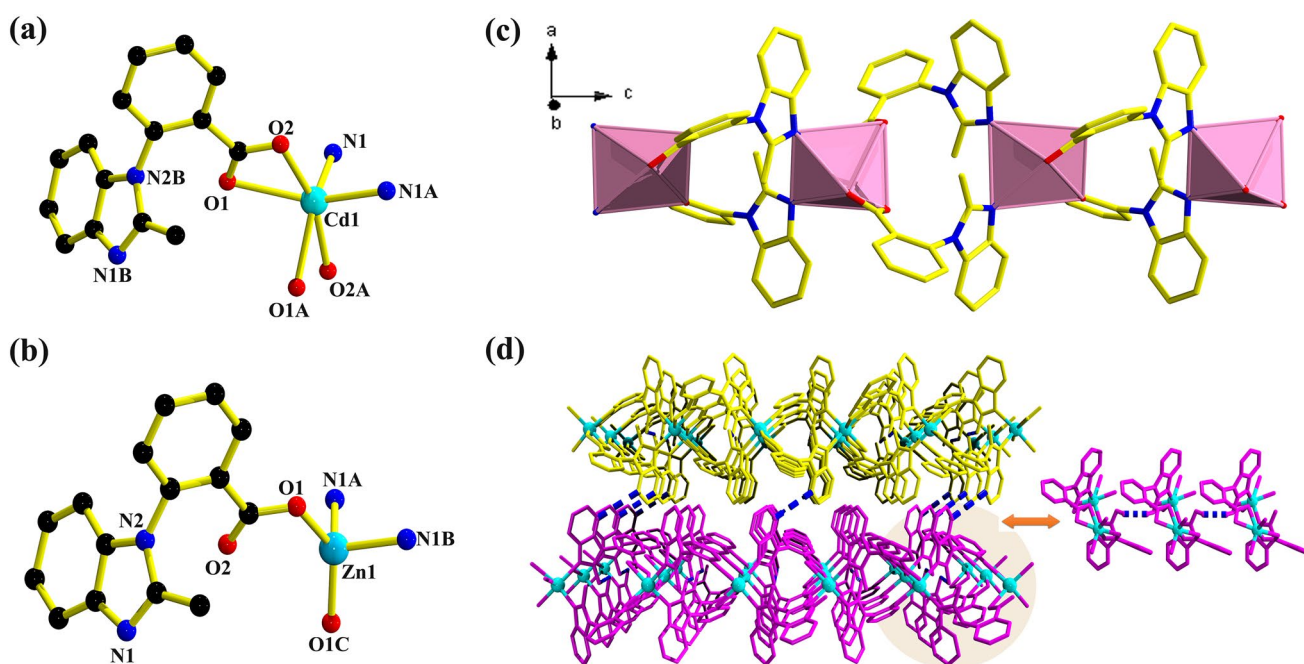


Fig. 1 **a** The coordination environment around Cd(II) ion in (**1**) Symmetry mode: $A=1/2-x, 1/2-y, z$. $B=x, 1/2-y, 1/2+z$. **b** The coordination environment around Zn(II) ions in (**2**) Symmetry mode: $A=x, 3/2-y, 1/2+z$. $B=1/2-x, y, 1/2+z$. $C=1/2-x, 3/2-y, z$

View of the 1D looped chain extending along the b axis. Cd, green; C, yellow; N, blue; O, red. **d** The 3D supramolecular framework formed by C–H...C hydrogen bond

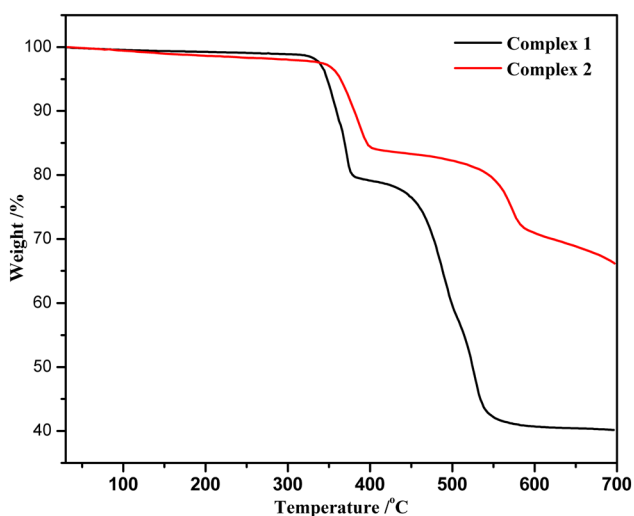


Fig. 2 TGA curves for **1** and **2**

450 nm, which has an overlap with the emission spectra of **1** and **2**, indicating the existence of resonance energy transfer (Fig. S5). As a result, the quenching mechanism caused by Fe^{3+} mainly depends on resonance energy transfer [44].

To assess the sensitivity of **1** and **2** toward Fe^{3+} in detail, varying concentrations of Fe^{3+} were introduced into emulsions of **1** and **2** dispersed in DMF and the emissive responses were monitored. The emission intensities

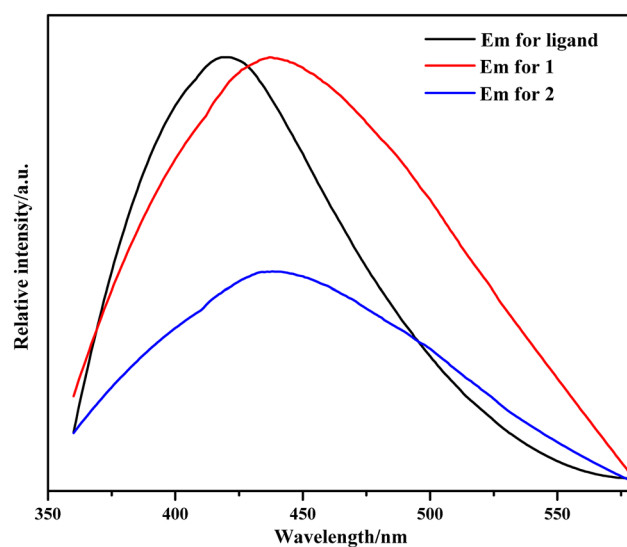


Fig. 3 Emission spectra of ligand, **1** and **2** in the solid state at room temperature

decrease gradually with increasing Fe^{3+} concentrations (Fig. 4b). The plot of I_0/I vs concentration of Fe^{3+} ion does not match with the Stern–Volmer equation, indicating the coexistence of the dynamic and static quenching processes, [45, 46] which can be well fitted by $I_0/I=5.22 \times \exp(c/0.74)-5.38$ for **1** and $I_0/I=1.63 \times \exp(c/0.61)-0.55$

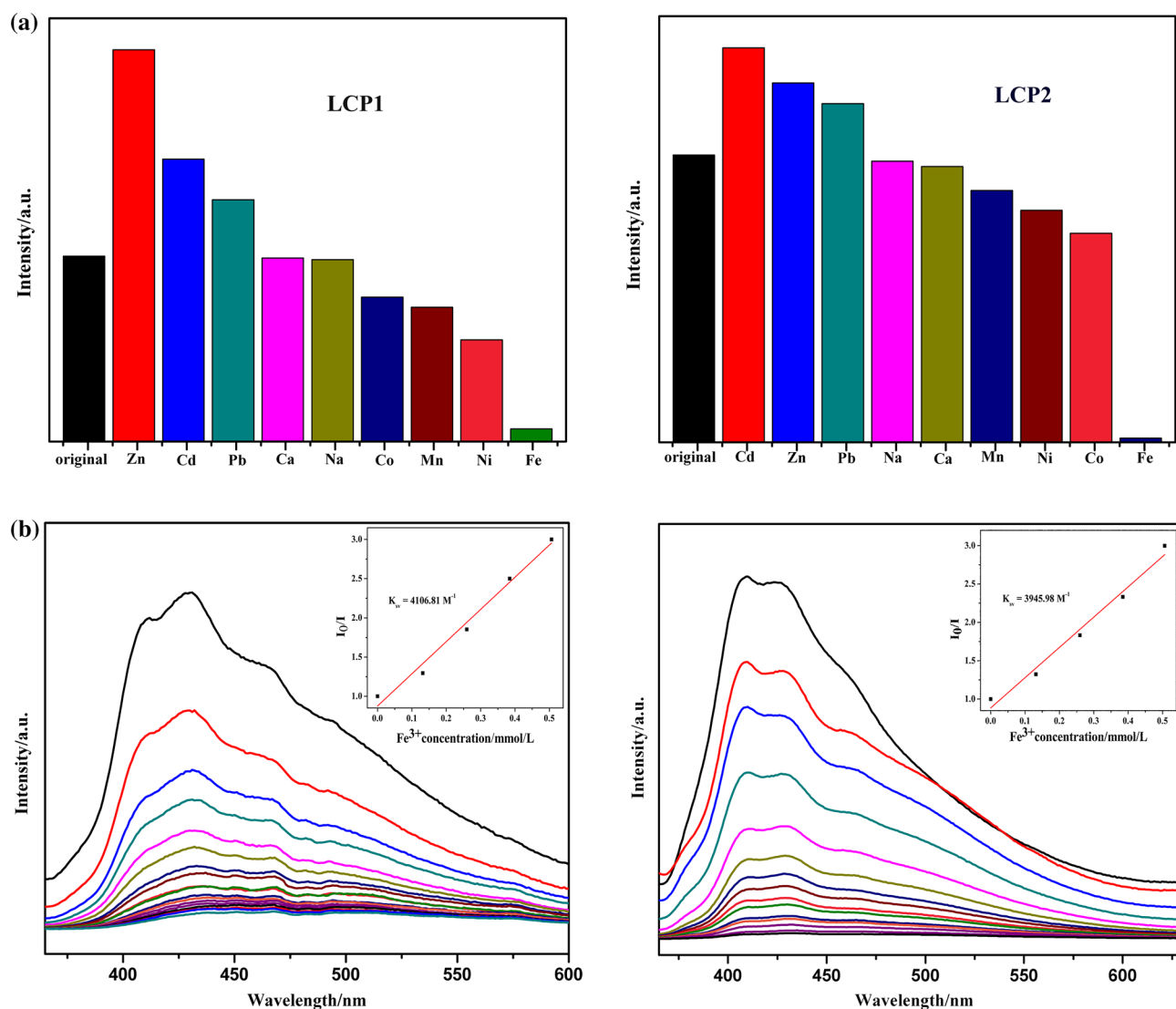


Fig. 4 **a** Room-temperature luminescent intensity of **1** and **2** at 435 nm in DMF suspension upon addition of various metal ions. **b** Fluorescence spectra of **1** (left) and **2** (right) in DMF with increasing

amounts of Fe³⁺. Insets: the linear correlation for the plot of I_0/I vs concentration of Fe³⁺ ions in low concentration range

for **2** (I_0 and I are the luminescent intensity of **1** and **2** in the absence and presence of Fe³⁺, respectively; and c is the molar concentration of Fe³⁺) (Fig. S6). Thereby, the quenching process completely depends on the concentration of Fe³⁺ ion. Meanwhile, this function in the range of 0–0.5 mmol/L conforms to a good linear correlation. As shown in Fig. 4b, the fluorescence intensity vs [Fe³⁺] insert plot can be linear-fitted into $I_0/I - 1 = K_{sv}[Fe^{3+}] - 0.12$ for **1** and $I_0/I - 1 = K_{sv}[Fe^{3+}] - 0.11$ for **2**, closed to the Stern–Volmer equation: $I_0/I - 1 = K_{sv}[M]$. ([M] is the metal ion molar concentration; K_{sv} is the quenching efficiency to quantitatively evaluate the performance of LCPs as sensor.) Base on the experimental data, the K_{sv} value is calculated to be 4106.81 L mol for **1** and 3945.98 L mol for **2**. Both K_{sv}

values are comparable to those in well-designed solution base organic complexes for sensing of Fe³⁺ (typical K_{sv} of about 10⁴ L/mol) [47]. The results indicate that **1** and **2** can be used as promising luminescence sensors for Fe³⁺ ions.

4 Conclusion

In summary, under solvothermal conditions, we have successfully synthesized two new 1D looped LCPs **1** and **2** with different coordination modes of carboxyl based on 2-(2-methyl-benzimidazole-1-yl)-benzoic acid (HL) ligand. Both LCPs are thermally stable up to 330 and 350 °C, and exhibit strong luminescence emissions in the

solid state and in a DMF suspension at room temperature. The experimental results and data show that **1** and **2** display high selectivity and quantitative detection for Fe³⁺ through fluorescence quenching, suggesting that both LCPs may be used as luminescent probes for Fe³⁺.

Acknowledgements This work was supported by the NSF of China (No. 21673173, 21272184, 21572177, 21371142, 21531007, 21103137 and J1210057), the NSF of Shaanxi Province of China (No. 2016JZ004 and 2015JZ003), the Xi'an City Science and Technology Project (No. CXY1511(3)), the Northwest University Science Foundation for Postgraduate Students (No. YZZ14052 and YZZ15040) and the Chinese National Innovation Experiment Program for University Students (No. 201510697004) for financial support.

References

- M. Zheng, H.Q. Tan, Z.G. Xie, L.G. Zhang, X.B. Jing, Z.C. Sun, *Appl. Mater. Interfaces* **5**, 1078–1083 (2013)
- Y.H. Hung, A.I. Bush, R.A. Cherny, *J. Biol. Inorg. Chem.* **15**, 61–76 (2010)
- Z.O. Tesfaldet, J.F. van Staden, R.I. Stefan, *Talanta* **64**, 1189–1195 (2004)
- A. Ohashi, H. Ito, C. Kanai, H. Imura, K. Ohashi, *Talanta* **65**, 525–530 (2005)
- Y. Rachuri, B. Parmar, K.K. Bishta, E. Suresh, *Dalton Trans.* **45**, 7881–7892 (2016)
- X. Shen, B. Yan, *RSC Adv.* **6**, 28165–28170 (2016)
- L. Wang, Z.Q. Yao, G.J. Ren, S.D. Han, T.L. Hu, X.H. Bu, *Inorg. Chem. Commun.* **65**, 9–12 (2016)
- L.L. Wen, X.F. Zheng, K.L. Lv, C.G. Wang, X.Y. Xu, *Inorg. Chem.* **54**, 7133–7135 (2015)
- X.D. Wang, O.S. Wolfbeis, R. Meier, *Chem. Soc. Rev.* **42**, 7834–7869 (2013)
- Z.C. Hu, B.J. Deibert, J. Li, *Chem. Soc. Rev.* **43**, 5815–5840 (2014)
- J. Rocha, L.D. Carlos, F.A.A. Paz, D. Ananias, *Chem. Soc. Rev.* **40**, 926 (2011)
- X.D. Wang, O.S. Wolfbeis, R.J. Meier, *Chem. Soc. Rev.* **42**, 7834–7869 (2013)
- L. Basabe-Desmonts, D.N. Reinhoudt, M. Crego-Calama, *Chem. Soc. Rev.* **36**, 993–1017 (2007)
- Y. Xiao, Y. Cui, Q. Zheng, S. Xiang, G. Qian, B. Chen, *Chem. Commun.* **46**, 5503–5505 (2010)
- Z. Hao, X. Song, M. Zhu, X. Meng, S. Zhao, S. Su, W. Yang, S. Song, H. Zhang, *J. Mater. Chem. A* **1**, 11043–11050 (2013)
- J.M. Zhou, W. Shi, H.M. Li, H. Li, P.J. Cheng, *Phys. Chem. C* **118**, 416–426 (2014)
- H.B. Xu, S.H. Zhou, L.L. Xiao, H.H. Wang, S. Li, Q.J. Yuan, *Mater. Chem.* **3**, 291–297 (2015)
- P.Y. Wu, Y.H. Liu, Y. Liu, J.R. Wang, Y. Li, W. Liu, J. Wang, *Inorg. Chem.* **54**, 11046–11048 (2015)
- B.B. Kang, N. Wei, Z.B. Han, *RSC Adv.* **5**, 1605–1611 (2015)
- F.A.S. Chipem, S.K. Behera, G. Krishnamoorthy, *Sens. Actuators B* **191**, 727–733 (2014)
- G.J. Barbante, P.S. Francis, C.F. Hogan, P.R. Kheradmand, D.J.D. Wilson, P.J. Barnard, *Inorg. Chem.* **52**, 7448–7459 (2013)
- T. Wen, D.X. Zhang, J. Liu, R. Lin, J. Zhang, *Chem. Commun.* **49**, 5660–5662 (2013)
- J. Li, C. C. Ji, L. F. Huang, Y. Z. Li, H. G. Zheng, *Inorg. Chem. Acta* **371**, 27–35 (2011)
- L.M. Fan, W.L. Fan, B. Li, X.Z. Liu, X. Zhao, X.T. Zhang, *RSC Adv.* **5**, 14897–14905 (2015)
- J. Yang, G.D. Xie, X.F. Chen, D. Wu, X.M. Lin, G. Zhang, Y.P. Cai, *CrystEngComm* **17**, 1326 (2015)
- Q.Q. Li, Y.F. Kang, C.Y. Ren, G.P. Yang, Q. Liu, P. Liu, Y.Y. Wang, *CrystEngComm* **17**, 775 (2015)
- T. Alexander, P. Alexander, M. Stefan, W. Gerhard, M. Ingo, S. Thomas, *Inorg. Chem.* **53**, 6346–6356 (2014)
- G.M. Sheldrick, *SHELXL-97, Program for the Refinement of the Crystal Structures*, University of Göttingen, Göttingen, (1997)
- G.M. Sheldrick, *SHELXTL Reference manual version 5.1 (Bruker AXS)*, Madison (1997)
- H. W. Kuai, X. C. Cheng, X. H. Z. Zhu, *Naturforsch* **68b**, 789–796 (2013)
- T. Li, X.J. Hong, X. Liu, R. Chen, Q.G. Zhan, X. Xu, Y.P. Cai, *CrystEngComm* **16**, 3883 (2014)
- R. Mishra, M. Ahmad, M. RTripathi, *Polyhedron* **50**, 22–30 (2013)
- S. Mukherjee, D. Samanta, S.P. Mukherjee, *Cryst. Growth Des.* **13**, 5335–5343 (2013)
- R. Luo, H. Xu, H.X. Gu, X. Wang, Y. Xu, X. Shen, W.W. Bao, D.R. Zhu, *CrystEngComm* **16**, 784–796 (2014)
- D. Deya, S. Roy, R.N.D. Purkayastha, R. Pallepogu, P. McArdle, *J. Mol. Struct.* **1053**, 127–133 (2013)
- W.L. Liu, J.H. Yu, J.X. Jiang, L.M. Yuan, B. Xu, Q. Liu, B.T. Qu, G.Q. Zhang, C.G. Yan, *CrystEngComm* **13**, 2764 (2011)
- R. Mishra, M. Ahmad, M.R. Tripathi, *Polyhedron* **50**, 22–30 (2013)
- H. Erer, O.Z. Yeşilel, M. Arıcı, *Cryst. Growth Des.* **15**, 3201–3211 (2015)
- Z. Zhang, J.F. Ma, Y.Y. Liu, W.Q. Kan, J. Yang, *Cryst. Growth Des.* **13**, 4338–4348 (2013)
- Z.M. Ju, W. Yan, X.J. Gao, Z.Z. Shi, T. Wang, H.G. Zheng, *Cryst. Growth Des.* **16**(5), 2496–2503 (2016)
- J.X. Ma, X.F. Huang, X.Q. Song, S.W. Liu, *Chem. Eur. J.* **19**, 3590–3595 (2013)
- K. Jayaramulu, R.P. Narayanan, S.J. George, T.K. Maji, *Inorg. Chem.* **51**, 10089–10091 (2012)
- M.D. Allendorf, C.A. Bauer, R.K. Bhakta, R.J.T. Houk, *Chem. Soc. Rev.* **38**, 1330–1352 (2009)
- S.S. Nagarkar, B. Joarder, A.K. Chaudhari, S. Mukherjee, S.K. Ghosh, *Angew. Chem. Int. Ed.* **52**, 2881–2885 (2013)
- H. Xu, H.C. Hu, C.S. Cao, B. Zhao, *Inorg. Chem.* **54**, 4585–4587 (2015)
- G.P. Li, G. Liu, Y.Z. Li, L. Hou, Y.Y. Wang, *Inorg. Chem.* **55**(8), 3952–3959 (2016)
- S.K. Sahoo, D. Sharma, R.K. Bera, G. Crisponi, J.F. Callan, *Chem. Soc. Rev.* **41**, 7195–7227 (2012)